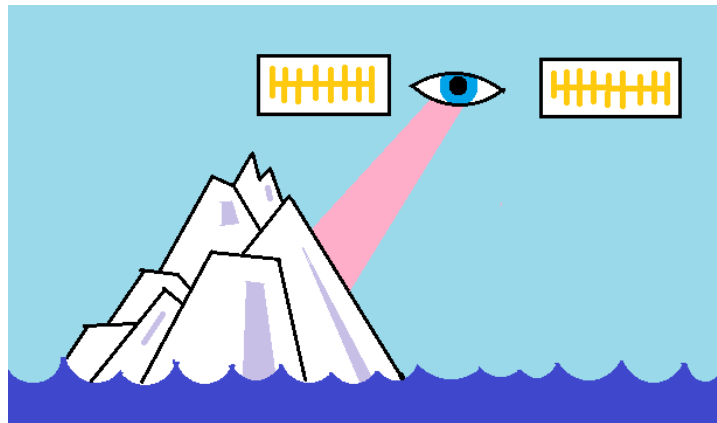


SEA ICE BRIGHTNESS TEMPERATURE AS A FUNCTION OF ICE THICKNESS

Part II: Computed curves
for
thermodynamically modelled ice profiles

Peter Mills

Peteysoft Foundation
1159 Meadowlane, Cumberland ON, K4C 1C3 Canada



Abstract

Ice thickness is an important variable for climate scientists and is still difficult to accurately determine from microwave radiometer measurements. There has been some success detecting the thickness of thin ice and with this in mind this study attempts to model the thickness-radiance relation of sea ice at frequencies employed by the Soil Moisture and Ocean Salinity (SMOS) radiometer and the Advanced Microwave Scanning Radiometer (AMSR): between 1.4 and 89 GHz. In the first part of the study, the salinity of the ice was determined by a pair of empirical relationships, while the temperature was determined by a thermodynamic model. Because the thermodynamic model can be used as a simple ice growth model, in this, second part, the salinities are determined by the growth model. Because the model uses two, constant-weather scenarios representing two extremes (“fall freeze-up” and “winter cold snap”), brine expulsion is modelled with a single correction-step founded on mass conservation. The growth model generates realistic salinity profiles, however it over-estimates the bulk salinity because gravity drainage is not accounted for. The results suggest that the formation of “skim” on the ice surface is important in determining the radiance signature of thin ice, especially at lower frequencies, while scattering is important mainly at higher frequencies but at all ice thicknesses.

1 Introduction

This study is a follow-up to a similar study (Mills and Heygster, 2011) in which the relationship between sea ice brightness temperature at microwave frequencies and ice thickness was examined. As noted in the previous study, several other works have demonstrated a relationship between ice thickness and SSM/I or AMSR-E brightness temperatures (Martin et al., 2004; Naoki et al., 2008; Kwok et al., 2007; Hwang et al., 2007) with at least one attempt to use this relationship for the purpose of ice thickness retrieval (Martin et al., 2004). To understand the relationship, determine it’s most likely functional form or forms and to set definite bounds on it would be of great value to ice remote sensing efforts. In particular, satellite retrieval of sea ice thickness in all weather conditions would be invaluable for climate scientists as it can help determine a number of important flux variables in the arctic regions such as heat and salt and fresh water. At present, the thickness of thin ice can be determined fairly accurately using infrared imagery, however this is quite cloud-sensitive, whereas microwave imagery is not.

In the first part, parameterised empirical relationships were used to relate bulk salinity to ice thickness and to determine the vertical salinity profile within the ice. In this second part, we will use a thermodynamic ice growth model, based primarily on first principles, to determine the salinity of the ice.

Table 1: Thermodynamic model parameters for the two weather scenarios

Parameter	Scenario	
	Fall freeze-up	Winter cold snap
Wind speed [m/s]	2.	10.
Air temperature [K]	270.	260.
Relative humidity	0.5	0.1
Cloud-cover	0.5	0.1
Insolation [W/m ²]	50.	0.

In Section 2 we will describe in detail the thermodynamic ice growth model, while in Section 3 we will present the results of the that model. Finally, in Section 4 we will apply the modelled profiles to the microwave emissivity simulation. All other parameters, in particular the emissivity model set up, will be the same as in the previous study and so will not be described.

2 Ice growth model

In the first part of the study (Mills and Heygster, 2011) a simple ice growth model based on constant weather scenarios was described. Here we apply the same model but with an extra step modelling brine expulsion added. These brine expulsion processes result from cooling of the ice sheet in the upper layers: because ice has a lower density than brine, as the ice grows downward, brine in the upper layers will freeze generating pressure in the remaining, more saline brine (Tucker et al., 1992).

Since we are using two, constant-weather scenarios—see Table 1—representing two possible extremes, there is no need to create an iterative, time-based, prognostic scheme, rather we take only ice thickness, h , in favour of time, t , as the dependent variable in the bulk of the model. The salinity profile is first modelled assuming no brine expulsion, then there is a “brine correction” step, in which mass conservation determines how much brine is lost based on the difference in temperature between the ice layer at first formation and at the final ice thickness.

The following equation relates the ice surface temperature to net heat flux:

$$hQ^* = k(T_w - T_s) \quad (1)$$

where T_w is the water temperature which is assumed to be constant at freezing (approximately -1.9° C at a water salinity of 35 psu), T_s is surface temperature and k is the thermal conductivity of the ice. The net heat flux

comprises the following components, with functional dependencies supplied:

$$Q^* = Q_E[e(T_s)] + Q_H(T_s) + Q_{SW}(T_s^4) + Q_{LW} \quad (2)$$

The terms on the RHS are, from left to right: latent heat, sensible heat, longwave and shortwave; $e(T)$ is the saturation vapour pressure. The first two terms are approximated with simple parameterisations while the longwave flux is based on the Stefan-Boltzmann law. The shortwave flux is calculated primarily from geometric considerations based on the position of the Earth relative to the Sun. The following inputs are required for the model: surface-wind speed, -humidity, -air temperature and -density (or pressure), cloud cover and date and time or insolation. (Cox and Weeks, 1988; Drucker et al., 2003; Yu and Lindsay, 2003) Inputs can be supplied to give a picture of the general weather conditions. For instance, fall freeze-up might be characterized by relatively mild temperatures, low winds, high humidity, high cloud cover and moderate insolation. By contrast, a winter cold snap would be characterized by low temperature, high winds, low humidity, clear conditions and little to no insolation. See Table 1. Equations (1) and (2) are solved with a numerical root-finding algorithm, specifically bisection (Press et al., 1992).

The model can also be used as a crude ice growth model. The rate of ice growth is:

$$g = \frac{Q^*}{L\rho_i} \quad (3)$$

where L is the latent heat of fusion for water and $\rho_i \approx 0.917 - 1.403 \times 10^{-4}T$ is the density of pure ice, which is a function of temperature. Empirical equations for determining the initial brine entrapment in sea ice have been derived by Cox and Weeks (1988) and Nakawo and Sinha (1981) and take the form:

$$S = S_0 f(g) \quad (4)$$

where S_0 is the salinity of the parent water and f is an empirical function of ice growth rate.

As shown in the previous report, if the salinities are left untouched, even as they move further from the bottom of the ice sheet, the model considerably over-estimates the bulk salinities. Using conservation of mass, we can correct for this in each layer based on the temperature differences between the thinner ice, when the layer is still forming, and the thicker ice as more layers have been added to the bottom. In the following, we go through all the relevant relationships needed to form the brine expulsion-correction model.

While we will not need it, the time, t , can be written as a function of ice thickness:

$$t(h) = \int_0^h g^{-1}(h') dh' \quad (5)$$

since the growth rate, g , is also a function of ice thickness. Because we assume constant weather conditions, temperature for a given point in the ice sheet is a monotonic function of ice age or thickness, hence there is no reason to construct a dynamical time series.

Due to freezing-point depression, the salinity of brine inclusions, S_b , is a function of temperature only. That is, greater salinity in the brine will lower its freezing point. As the brine cools, the water in it will freeze, increasing its salinity. Thus it is maintained at its freezing point at all times. We use the linear, piece-wise continuous model from Ulaby et al. (1986).

The total density at a given point in the ice is:

$$\rho = V_b \rho_b + (1 - V_b) \rho_i \quad (6)$$

where V_b is the relative brine volume, $\rho_b \approx 1 + 0.0008 S_b$ is the brine density (Cox and Weeks, 1983). Note that this neglects any air pockets that are usually included in the ice in addition to brine. These are particularly prevalent in older ice, but omitting them considerably simplifies the analysis.

The ice salinity is further related to the brine salinity as follows:

$$S = S_b \frac{\rho_b}{\rho} \quad (7)$$

From equations (6) and (7) we can solve for the relative brine volume, V_b :

$$V_b = \frac{S \rho_i}{S_b \rho_b - S(\rho_b + \rho_i)} \quad (8)$$

We assume that the ice is in thermodynamic equilibrium and the thermal conductivity is roughly constant throughout. Thus, the temperature of the ice sheet at depth, z , and thickness, h , is given by interpolating between the surface temperature, T_s and the water temperature, T_w :

$$T(h, z) = T_w + [T_s(h) - T_w]z/h \quad (9)$$

From this we can calculate the density of the ice sheet as a function of ice thickness and ice depth: $\rho(h, z)$. The relative change in volume, δv , is given as:

$$\delta v = (\rho/\rho_0 - 1) \quad (10)$$

where $\rho_0(h) = \rho(h, h)$ is the density of the ice layer as it is first forming. Since the amount of mass must remain constant, and since we assume there are no cavities in the ice, so must the volume remain constant, therefore we can determine how much material is ejected from the ice sheet. We assume that only brine is ejected, provided there is enough, thus:

$$\delta m = \begin{cases} \rho_b \delta v; & \delta v \leq V_b \\ \rho_b V_b + \rho_i (\delta v - V_b); & \delta v > V_b \end{cases} \quad (11)$$

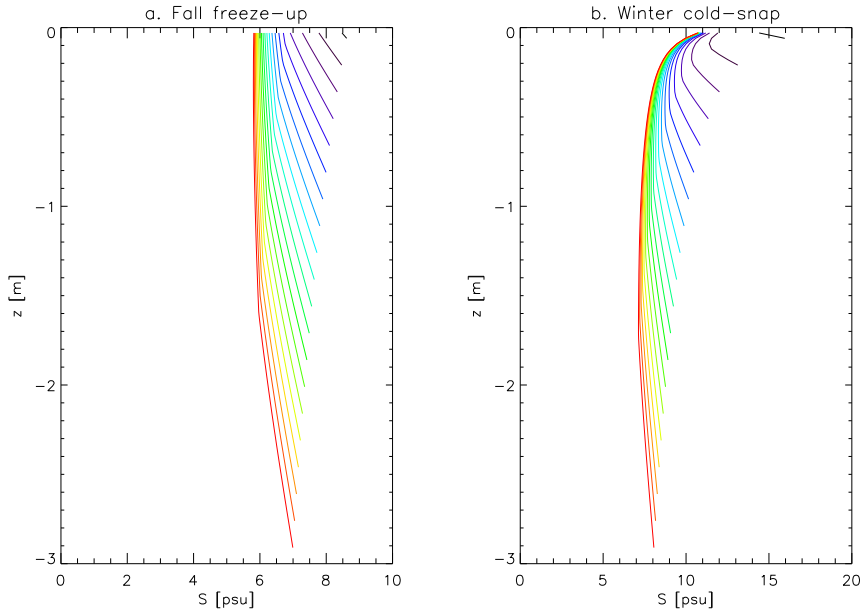


Figure 1: Modelled salinity profiles for different ice thicknesses and two weather scenarios: “fall freeze-up” and “winter cold-snap”; see Table 1.

is the relative change in mass or relative mass loss. It follows that the corrected brine volume is given as:

$$V_b^{(\text{new})} = \begin{cases} V_b - \delta v; & \delta v < V_b \\ 0; & \delta v \geq V_b \end{cases} \quad (12)$$

from which we can solve for the corrected salinity using Equation (8).

3 Growth model results

Results for the “fall freeze-up” and “winter cold-snap” scenarios are shown in Figures 1(a) and (b), respectively. Qualitatively, at least, these salinity profiles are quite realistic: thin-ice profiles for the cold-weather scenario show the characteristic, ‘C’-shape typical of young ice (Eicken, 1992), while the thicker, older ice has a flatter profile (Tucker et al., 1992). For the warm-weather scenario, the profiles are altogether flatter, which is typical of low-salinity ice (Granskog et al., 2006).

Bulk salinity as a function of thickness are shown in Figure 2, while thickness as a function of time is shown in Figure 3. There are two versions of the growth model salinities: “with skim” and “without skim”, both of which deserve some explanation. The brine that has been ejected has to go somewhere. In the first case, we assume that exactly half of it collects on

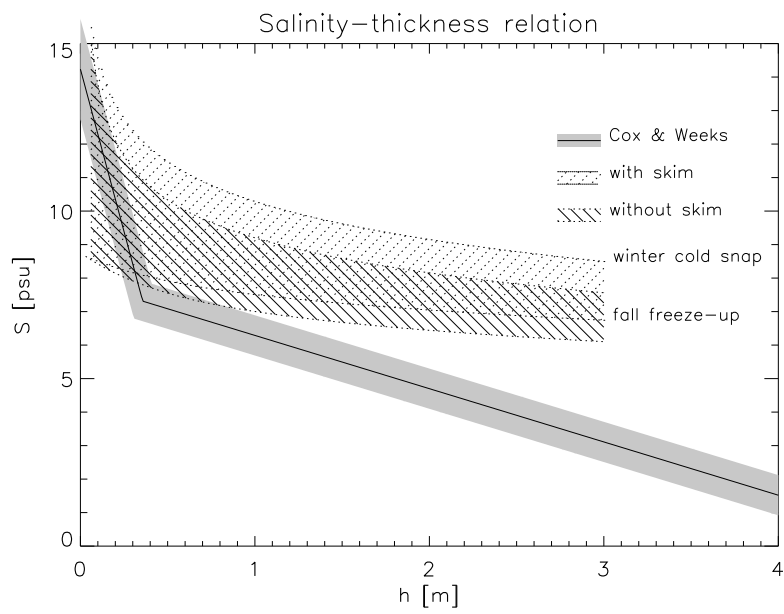


Figure 2: Modelled versus empirical salinity-thickness relationships. Solid shading shows the residuals for the Cox and Weeks (1974) models. The areas in between the two weather scenarios are hatched. See text for an explanation of the difference between “with skim” and “without skim.”

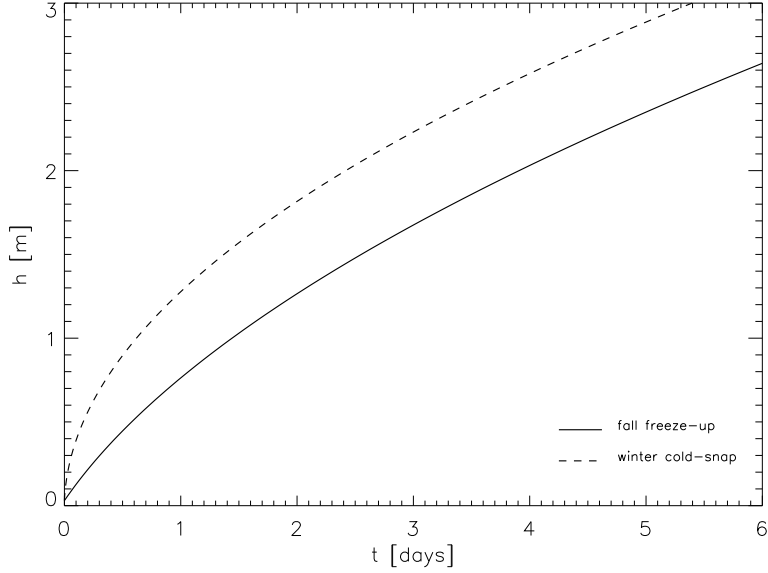


Figure 3: Ice thickness as a function of time for the two contant- weather scenarios.

top of the ice sheet as “skim”, while in the second case, we assume that all of it is ejected downward, into the ocean.

We need to calculate both the salinity of the skim, and its thickness for further use in the emissivity model. Following Equation (7), the lost salinity in each layer is:

$$S_{\text{lost}} = \begin{cases} S_b \rho_b \delta v / \rho; & \delta v \leq V_b \\ S_b \rho_b V_b / \rho; & \delta v > V_b \end{cases} \quad (13)$$

The total mass loss is given as:

$$\delta m_{\text{total}} = \int_0^h \delta m dz \quad (14)$$

thus the salinity of the skim is calculated:

$$S_{\text{skim}} = \frac{1}{\delta m_{\text{total}}} \int_0^h S_{\text{lost}} \delta m dz \quad (15)$$

Assuming that the skim is at the temperature of the top layer, we can compute the density of the skim, ρ_{skim} , from Equations (8), then (6), from which follows its thickness:

$$\delta z_{\text{skim}} = \frac{\delta m_{\text{total}}}{2\rho_{\text{skim}}} \quad (16)$$

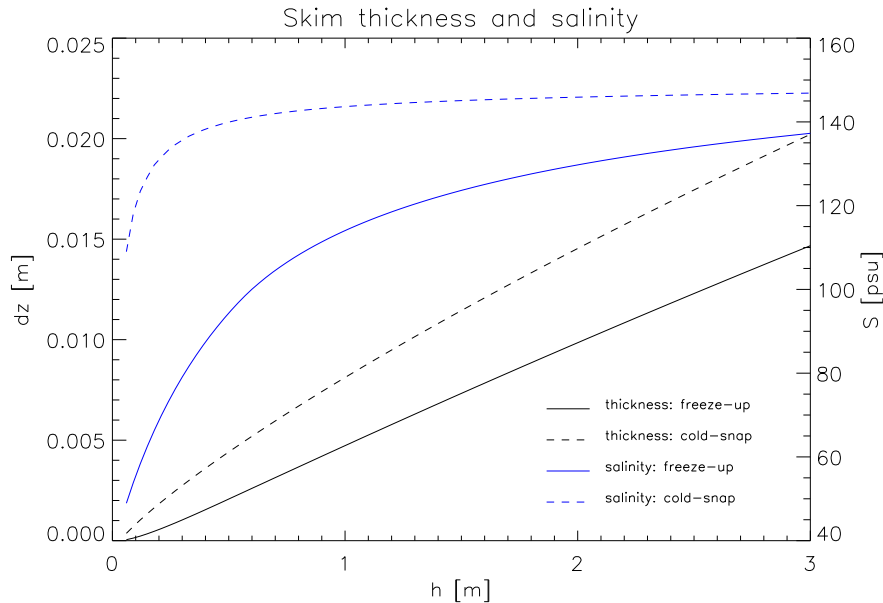


Figure 4: Thickness and salinity of “skim” layer.

Properties of the modelled skim layer are shown in Figure 4.

Note that even if all the ejected brine is lost from the ice sheet, the model still over-predicts the salinities in relation to the Cox and Weeks model, especially at deeper ice thicknesses. The reason for the discrepancy is that brine drainage has not been included in the growth model: as the ice ages, brine will drain through vertical channels. Still, we hope that feeding these results to the emissivity models will nonetheless provide some insight. For one thing, the salinity profile is different; also, there are more emissivity variations in thinner ice, where the model is more accurate.

4 Results

Here the final brightness temperature-thickness relations are presented. In this second part, the error bounds have also been calculated using a Monte Carlo or “boot-strapping” method (Press et al., 1992) by first varying the constant weather scenario between the two extremes presented in Table 1 to produce 100 sets of profiles for different ice thicknesses, then using the error bounds in the effective permittivity model to vary the effective permittivities over 100 additional trials, generating 10000 trials total. Uniform deviates (“white” noise) are used to vary the weather parameters while normal deviates (Gaussian noise) are used to vary the permittivities.

In the first set of graphs, Figure 5, neither the skim layer nor the scatter-

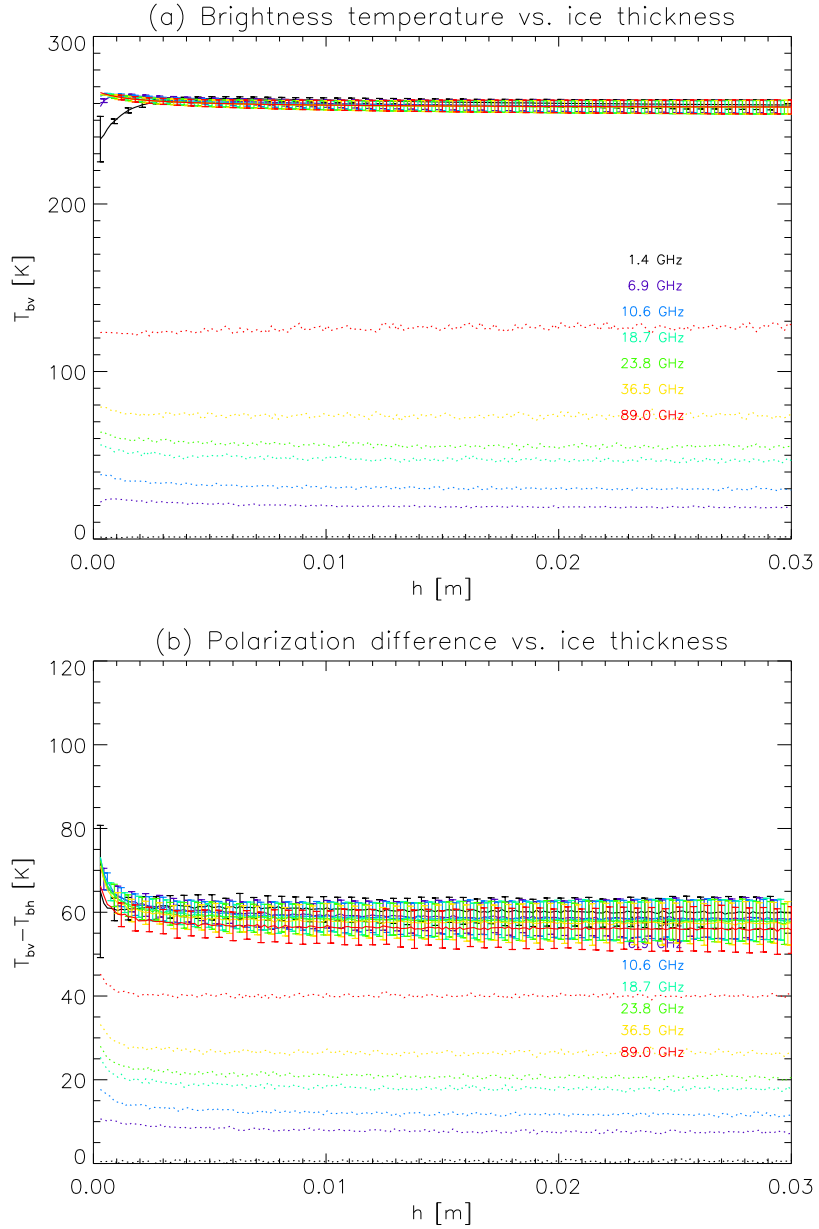


Figure 5: Modelled brightness temperature as a function of ice thickness based on modelled ice profiles, not including skin. Solid lines show model results neglecting scattering, while dotted lines show the computed scattering component.

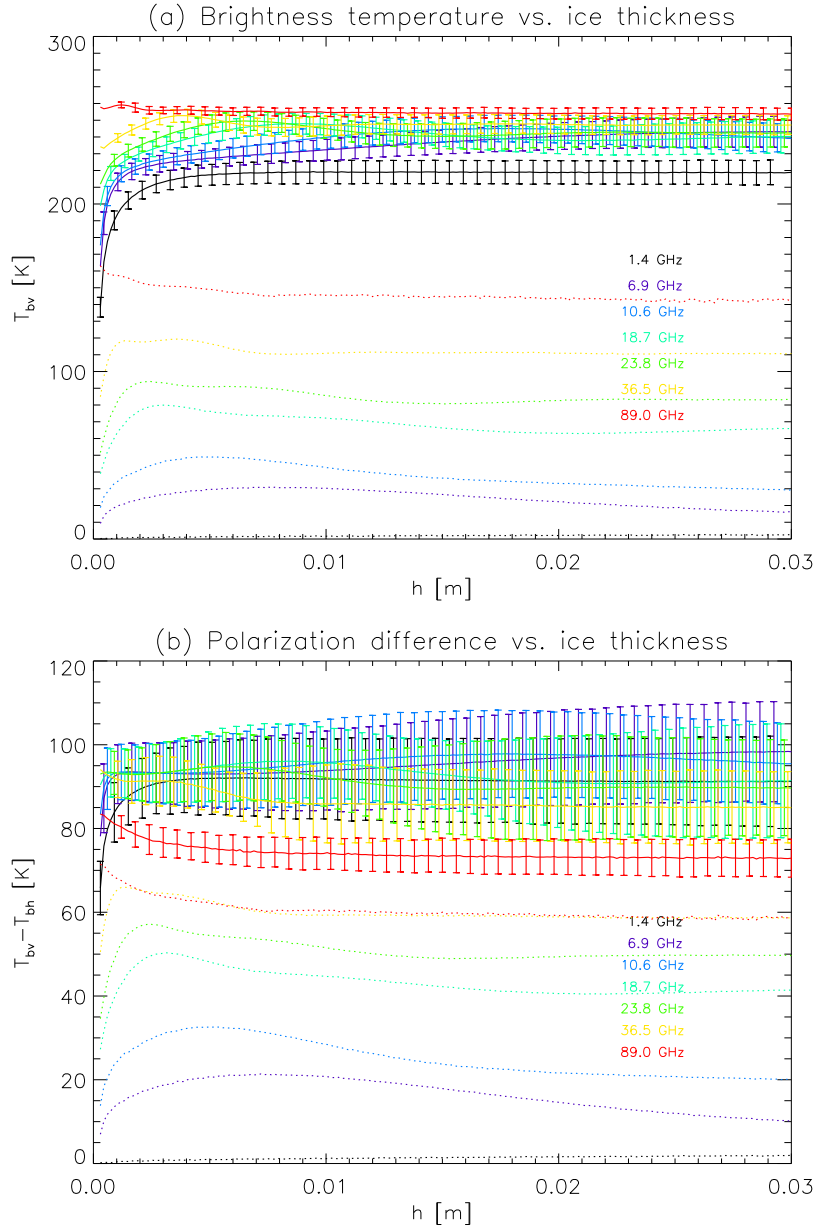


Figure 6: Modelled brightness temperature as a function of ice thickness based on modelled ice profiles, including skim. Solid lines show model results neglecting scattering, while dotted lines show the computed scattering component.

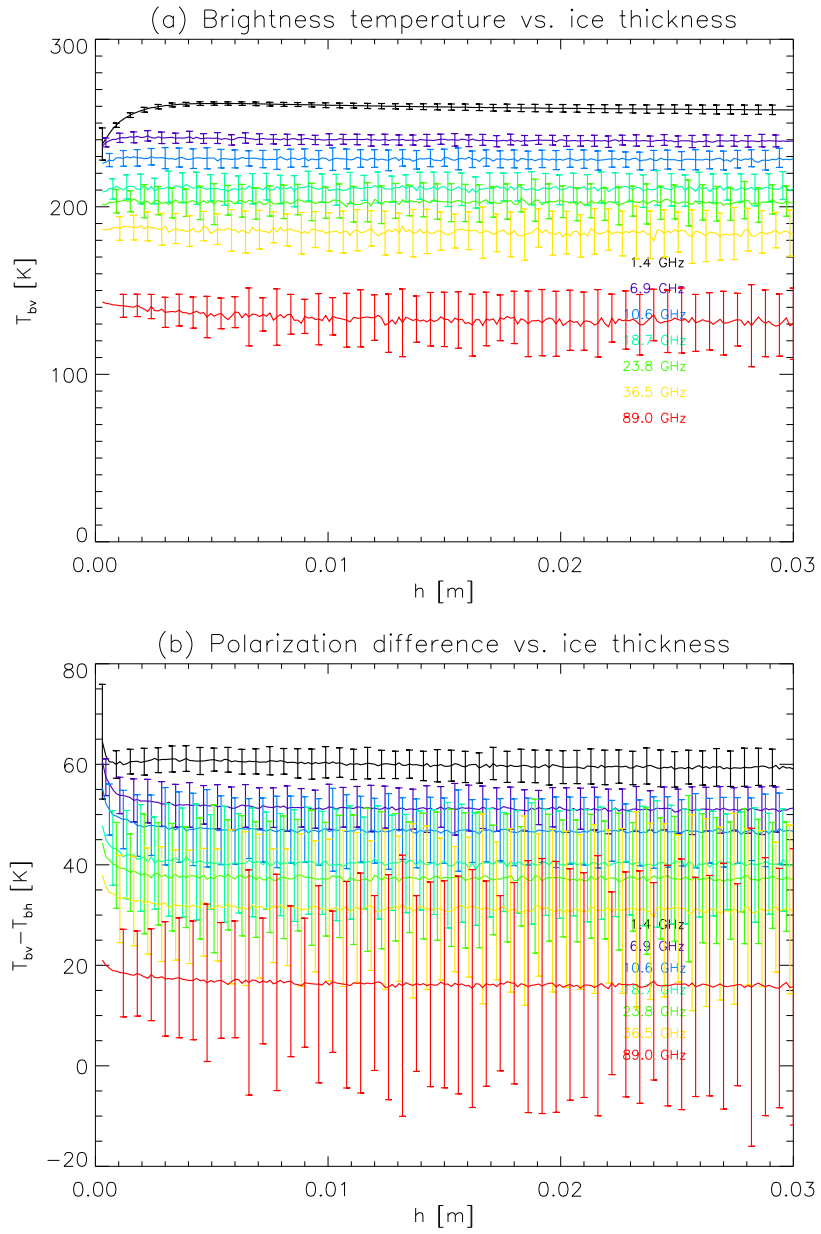


Figure 7: Modelled brightness temperature as a function of ice thickness based on modelled ice profiles, not including skim. Scattering has been included.

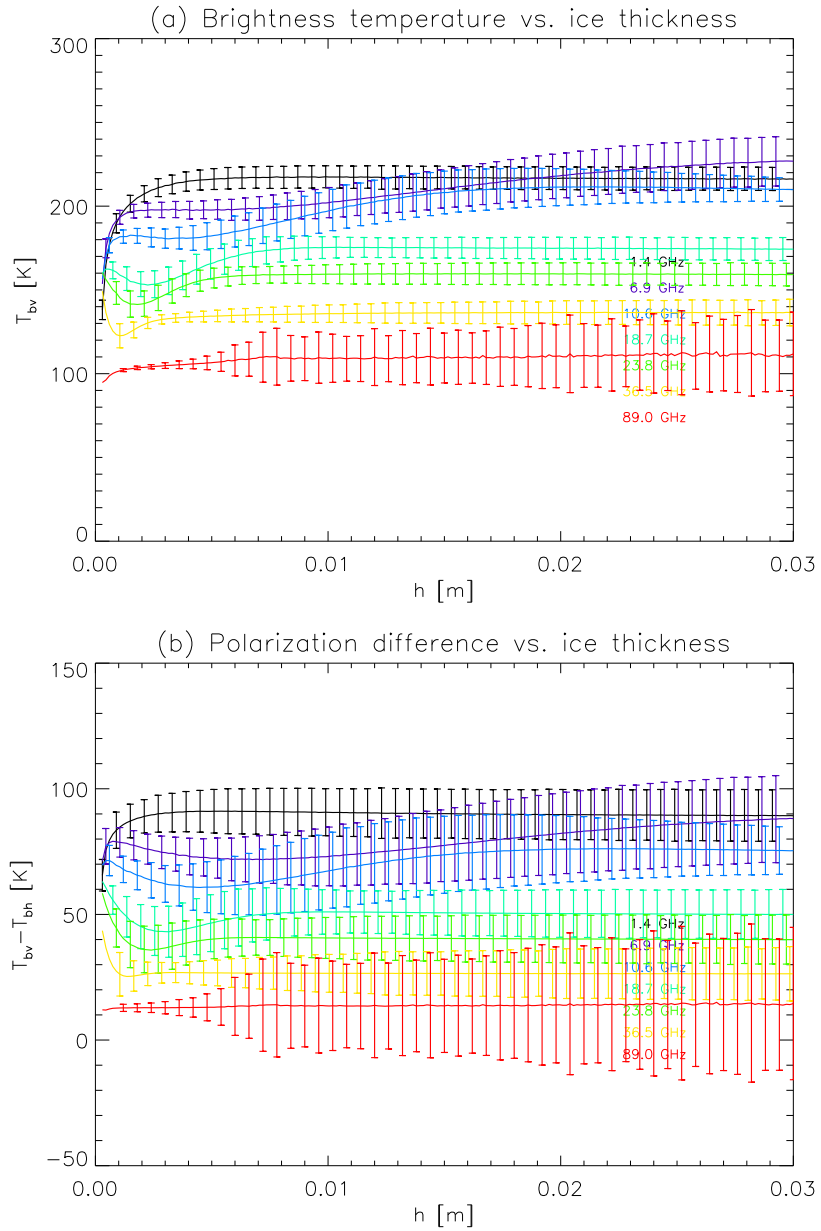


Figure 8: Modelled brightness temperature as a function of ice thickness based on modelled ice profiles, including skim. Scattering has been included.

ing component has been included in the emissivity calculations. The scattering components, however, have been graphed alongside the non-scattering components. The second set of graphs, Figure 6, is the same as the first, except the skim layer has been included. In the third set of graphs, Figure 7, the scattering and non-scattering components have been added together for the simulations not including skim. The fourth set of graphs, Figure 8, is the same as the third, except the skim layer has been included.

One of the most striking things about these results is how uniform the brightness temperatures are in Figure 5, both for different ice thicknesses and for different frequencies. Only the lowest frequency shows a slight dip at the thinnest ice thicknesses because of transparency: the water “shows through.” Even with the addition of skim in Figure 6, the brightness temperatures are still surprisingly uniform. Skim is one factor that is rarely included in either ice growth or ice emissivity models. Because of its high liquid and high saline content, it will be both highly reflective and highly absorbant, although because it is usually a very thin layer, it may still be quite translucent. Thus its presence will tend to lower the brightness temperature of the ice because it reflects the much cooler (as little as 3 K on clear days) sky, as well as increase the polarization difference because of its higher real permittivity. These results show a fairly uniform depression/increase in brightness temperature/polarization difference, but because the modelled skim does not drain as it would on real ice, the actual tendency would apply only to new and thin ice.

The lower the frequency, the more both the real and the imaginary permittivity increase with brine volume (see Figure 10 from Part I (Mills and Heygster, 2011)), thus the effect of the skim is more pronounced at lower frequencies. Therefore, at lower frequencies, the characteristic lowered brightness temperature and raised polarization difference of new and thin ice is caused by the accumulation of skim. At higher frequencies, this is caused by scattering. The results here show that scattering increases the variability of the signal especially at higher frequencies and especially at higher ice thicknesses. Note that skim also increases the variability, but more so at lower frequencies. In real ice we would expect the effect of scattering to be more pronounced in thin rather than thick ice, and this does show up somewhat in the model results, but only when skim is included.

5 Summary and conclusions

A simple thermodynamic model was used to simulate ice growth for constant weather scenarios ranging between two extremes. This model takes into account both heat conduction and brine expulsion without the need to construct a dynamical time series, but neglects brine drainage. The resulting temperature and salinity profiles are fed to the Microwave Emis-

sion Model of Layered Snowpack (MEMLS) to determine the functional dependence of microwave radiance on ice thickness. The resulting salinity profiles and consequent salinity-thickness relation, as well as the simulated brightness-temperature-thickness relations, are quite realistic. The following observations may be noted: 1. Without a layer of “skim” collected on top of the ice and neglecting scattering, the brightness temperatures of the ice are surprisingly uniform, both over different frequencies and different ice thicknesses. Thus, variations in emissivity must be attributed to other, secondary factors which we describe below.

The presence of skim, a semi-liquid collection of brine and ice that accumulates on top of ice sheets due to brine expulsion, is neglected in most ice growth and emissivity models. Here the skim has been modelled as simply the aggregate of exactly half the brine that has been expelled from the ice sheet. 2. Because of its high opacity and high real permittivity, the presence of skim will tend to lower the brightness temperature and increase the polarization difference. This effect is more pronounced at lower frequencies and at thinner ice thickness, but the latter effect is not present because the growth model neglects brine drainage. 3. Thus, the lower brightness temperature and higher polarization difference characteristic of new and thin ice is primarily caused by the presence of skim.

4. Finally, scattering will have a strong effect at higher frequencies. 5. Skim in particular will scatter strongly. 6. Thus, lower brightness temperature and higher polarization in thin and new ice and lower brightness temperature and higher polarization difference in general at higher frequencies is caused by scattering, especially by the skim. 7. Both the presence of skim and scattering will tend to increase the variability of the signal.

Both ice growth and the interaction of sea ice with electromagnetic radiation are extremely complex processes with many different facets. They are very difficult to model effectively. Moreover, since all of: the microstructural properties, the macroscopic configuration, the relative composition, will affect the emitted microwave signal, and all these can change with the prevailing weather conditions, ice growth and ice emissivity cannot be treated in isolation. Figures 1 and 2 in Part I (Mills and Heygster, 2011) give some idea of the complexity of the problem.

We believe the contents of this and the previous report represent an advance in the state-of-the-art, however there are still many limitations in the current effort. 1. The ice growth model over-estimates salinity and the size of the skim layer at high ice thicknesses because it neglects brine-drainage. 2. Scattering is too high and too variable at high ice thicknesses. The scattering model is fairly crude and likely inaccurate, not least of which because the correlation length are estimated by a simple, ad-hoc assumption. 3. The complex permittivities do not take into account ice microstructural properties, they do not have a comprehensive physical explanation and they are not validated at higher frequencies. As a first step, there are many new

directions that the semi-empirical permittivity model could be taken in. A Debye relaxation curve for different brine volumes, for instance, is suggested by the strong, simple dependence on frequency.

References

- Cox, G. and Weeks, W. (1983). Equations for determining the gas and brine volumes in sea-ice samples. *Journal of Glaciology*, 29(102):306–316.
- Cox, G. and Weeks, W. (1988). Numerical simulations of the profile properties of undeformed first-year sea ice during the growth season. *Journal of Geophysical Research*, 93(C10):12499–12460.
- Cox, G. F. N. and Weeks, W. F. (1974). Salinity variations in sea ice. *Journal of Glaciology*, 13(67):109–120.
- Drucker, R., Martin, S., and Moritz, R. (2003). Observations of ice thickness and frazil ice in the St. Lawrence Island polynya from satellite imagery, upward looking sonar, and salinity/temperature moorings. *Journal of Geophysical Research*, 108(C5).
- Eicken, H. (1992). Salinity Profiles of Antarctic Sea ice: Field Data and Model Results. *Journal of Geophysical Research*, 97(C10):15545–15557.
- Granskog, M., Kaartokallio, H., Kuosa, H., Thomas, D. N., and Vainio, J. (2006). Sea ice in the Baltic Sea—A review. *Estuarine, Coastal and Shelf Science*, 70:145–160.
- Hwang, B. J., Ehn, J. K., Barber, D. G., Galley, R., and Grenfell, T. C. (2007). Investigations of newly formed sea ice in the Cape Bathurst polynya: 2. Microwave emission. *Journal of Geophysical Research*, 112(C05003).
- Kwok, R., Comiso, J., Martin, S., and Drucker, R. (2007). Ross Sea polynyas: Response of ice concentration retrievals to large areas of thin ice. *Journal of Geophysical Research*, 112(C12012).
- Martin, S., Drucker, R., Kwok, R., and Holt, B. (2004). Estimation of the thin ice thickness and heat flux for the Chukchi Sea Alaskan coast polynya from Special Sensor Microwave Imager data, 1990-2001. *Journal of Geophysical Research*, 109(C10012).
- Mills, P. and Heygster, G. (2011). Sea ice emissivity as a function of ice thickness: computed curves for AMSR-E and SMOS (frequencies from 1.4 to 89 GHz). Technical Report DFG project HE-1746-15, University of Bremen.

- Nakawo, M. and Sinha, N. K. (1981). Growth rate and salinity profile of first-year sea ice in the high arctic. *Journal of Glaciology*, 27(96):315–330.
- Naoki, K., Ukita, J., Nishio, F., Nakayama, M., Comiso, J. C., and Gasiewski, A. (2008). Thin sea ice thickness as inferred from passive microwave and in situ observations. *Journal of Geophysical Research*, 113(C02S16).
- Press, W. H., Teukolsky, S. A., Vetterling, W. T., and Flannery, B. P. (1992). *Numerical Recipes in C*. Cambridge University Press, second edition.
- Tucker, W. B., Perovich, D. K., Gow, A. J., Weeks, W. F., and Drinkwater, M. R. (1992). Physical Properties of Sea Ice Relevant to Remote Sensing. In *Microwave Remote Sensing of Sea Ice*, number 68 in Geophysical Monographs, chapter 2, pages 9–28. American Geophysical Union.
- Ulaby, F. T., Moore, R. K., and Fung, A. K., editors (1986). *Microwave Remote Sensing: Active and Passive, Volume III, From Theory to Applications*. Artech House, Norwood, MA.
- Yu, Y. and Lindsay, R. W. (2003). Comparison of thin ice thickness derived from RADARSAT Geophysical Processor System and Advanced Very High Resolution Radiometer data sets. *Journal of Geophysical Research*, 108(C12).

This figure "creepyice.png" is available in "png" format from:

<http://arxiv.org/ps/1202.6567v2>